Progress in Nuclear Energy 53 (2011) 1066–1072

Contents lists available at ScienceDirect

Progress in Nuclear Energy

journal homepage: www.elsevier.com/locate/pnucene

Corrosion behavior of heat-treated Fe–Al coated steel in lead–bismuth eutectic under loading

Eriko Yamaki-Irisawa [a,*], Shunichi Numata [a], Minoru Takahashi [b]

[a] Department of Nuclear Engineering, Tokyo Institute of Technology, N1-18, 2-12-1, Ookayama, Meguro-ku, Tokyo 152-8550, Japan
[b] Research Laboratory for Nuclear Reactors, Tokyo Institute of Technology, N1-18, 2-12-1, Ookayama, Meguro-ku, Tokyo 152-8550, Japan

ARTICLE INFO

Article history:
Received 29 October 2010
Received in revised form
12 May 2011
Accepted 13 May 2011

Keywords:
Lead-bismuth eutectic
316SS
Corrosion
Fe–Al
Coating
Stress

ABSTRACT

A protective surface alloy coating on steel surfaces can prevent steels from the heavy LBE corrosion in the LBE cooled reactor. Especially, Fe–Al alloy coating on a steel surface is effective for corrosion resistance in LBE due to the self-healing of a thin and stable Al oxide layer on the surface of the coating layer. In order to investigate the utility of the coating layer under the stress due to the hydrodynamic and thermal stress induced in the practical system. The Fe–Al coated 316SS, which was heat-treated after the coating process, was immersed in the stagnant LBE at 650 °C for 250 h with loading to investigate the corrosion behavior of the specimen with the bending stress. The Fe–Al coating layer was not corroded because of the protection by Al oxide scale which was formed on the surface of the coating layer and the interface between the coating and the matrix during the heat treatment process. The coating layer cracked elastically. The LBE penetrated into the cracks and corroded the 316SS matrix and the pre-coating layer. The matrix exhibited the dissolution corrosion caused by the preferential dissolution of Ni and the oxidation forming the Fe oxide and Cr oxide. The coating layer is effective to reduce the surface of the matrix to be corroded by LBE, and can moderate the corrosion of the depth direction.

1. Introduction

Lead–bismuth eutectic (LBE) is one of candidate coolants for the fast breeder reactor (FBR) and a coolant and a spallation target material for the accelerator driven nuclear transmutation system (ADS). One of key issues for the use of the LBE in FBRs and the ADS is compatibility of structural steel materials with high temperature LBE. Steel materials are oxidized by the high temperature LBE at high oxygen concentration, while they are attacked by the high temperature LBE at low oxygen concentration due to the dissolution of metallic elements into the liquid LBE and the penetration of the liquid LBE into the material. An austenitic 316 type stainless steel (316SS) is one of candidates of the structural materials for the LBE cooled reactor. However, since Ni has high solubility to LBE, the austenitic 316 type stainless steel which contain about 10wt%Ni are damaged seriously caused by the preferential dissolution of Ni (Kurata et al., 2005).

In order to prevent the heavy LBE dissolution corrosion of the steel, it is a good method to prevent the steel surface from contacting with liquid LBE directly. A protective surface alloy coating on steel surfaces can reduce the damage to the steels caused by the preferential dissolution to LBE. Especially, Fe–Al alloy coating on a steel surface is effective for corrosion resistance in LBE due to the self-healing of a thin and stable Al oxide layer on the surface of the coating layer (Kurata et al., 2004). The Fe–Al alloy coating layer can protect steels from corrosion not only in LBE environment but also in gas atmosphere. Lui et al. reported that a metastable cubic alumina phase (θ-Al_2O_3) was formed in early stage of the oxidation process of the intermetallic coating surface of Fe-45at%Al which was made by the magnetron sputtering technique (Lui et al., 1998). As for the LBE environment, Rivai et al. reported that a stable aluminum oxide layer which prevented the penetration of LBE into steels was formed on the surface of the sputtering Fe–Al coating layer in static LBE at 700 °C (Rivai and Takahashi, 2008).

In the practical system, the structural materials are exposed not only to the corrosive LBE environment but also to the hydrodynamic and thermal stress environment. The hydrodynamic stress is induced by the heavy LBE flow, and the thermal stress is induced by the temperature distribution due to a nuclear heat generation. It is concerned that these environments may affect the integrity of the coating alloy layers, resulting in cracks of the coating layer and decrease in adhesion of the coating layer to a matrix. However, there are few reports on corrosion characteristics of steels with metallic Fe–Al coating layers in LBE under the mechanical stress.

* Corresponding author.
E-mail address: yamaki.e.aa@m.titech.ac.jp (E. Yamaki-Irisawa).

0149-1970/$ – see front matter © 2011 Elsevier Ltd. All rights reserved.
doi:10.1016/j.pnucene.2011.05.014

It's not clear what is happened after cracking of the coating layer and how the dissolution corrosion advance.

The 316 type stainless steel coated with Fe–Al alloy is corroded in LBE under mechanical stress after the heat treatment. In order to evaluate the effect of the protection by the coating layer when the coating crack, the corrosion and fracture behavior of the coating layer and the 316SS matrix with cracking of the coating layer.

2. Experimental method

2.1. Material

The austenitic 316 type stainless steel was used as a matrix of test specimens. The chemical composition of 316SS is listed in Table 1. The shape and sizes of the specimens are shown in Fig. 1. The thickness of the specimens is 0.5 mm.

The surface of 316SS matrix was polished with emery papers (up to #2400) and then with diamond paste of 1 μm before coating process. The heat treatment before the coating process was not performed. A coating layer was formed with a physical vapor deposition (PVD) method in an unbalanced magnetic field: the unbalanced magnetron sputtering (UBMS) method where Ar ions were increased by non-equilibrium magnetic fields for bombardment. Al and 304SS were used as sputtering targets, where the austenitic stainless steel 304SS was chosen instead of pure iron because of no influence on magnetic fields, which means that not only Fe but also Cr and Ni were coated. The specimen temperature was kept 330–350 °C during the coating process. Before the Fe–Al alloy coating process, Fe pre-coating was performed for 5 min using only the 304SS target. It was expected to inhibit inward diffusion of Al to the matrix and achieve good adhesion between the coating layer and the matrix by means of the Fe pre-coating, since the pre-coating layer had no large difference of chemical compositions from those of the matrix. The thickness of the pre-coating layer was approximately 1 μm. Fe–Al coating process was performed for 570 min with the same voltage to form the Fe–Al coating layer with a thickness of about 20 μm.

After the coating process, in order to remove the residual stress in the coating layer, the coated specimens were was heat-treated in Ar gas. First, the specimens were kept at 850 °C to keep the Fe–Al layer as Fe–Al (B2) phase for 8 h and next at 650 °C for 6 h.

2.2. Corrosion test under loading

The experimental apparatus is shown schematically in Fig. 2. The apparatus consists of the corrosion test section and the gas injection system for control of oxygen concentration in LBE. The corrosion test section consists of an electric heater, an alumina crucible for LBE, a specimen holder made of 316 stainless steel, an oxygen sensor and a loading device made of 316SS. Fresh LBE without the dissolution of metal impurities was used in each corrosion test to avoid the effect of dissolved metal elements on the corrosion. The concentrations of Ni and Cr in LBE before the corrosion test, which were obtained by ICP-MS, were 3.9×10^{-5} wt % and 1.9×10^{-6} wt% respectively. These values were lower than the solubilities of Ni and Cr in LBE at 650 °C (the Ni solubility is 4.6 wt% and the Cr solubility is 3.2×10^{-3} wt%). Oxygen concentration in the LBE was kept at low level in the test section by injecting a reduction gas of Ar-3%H_2 mixture into the liquid LBE directly from the gas injection system. The flow rate of the gas injection was 0.5 ml/min. Oxygen concentration was monitored by a zirconia solid electrolyte oxygen sensor with a reference electrode of oxygen-saturated Bi/Bi_2O_3 mixture.

Table 1
Chemical composition of 316SS (wt%).

Fe	Cr	Ni	Mo	Mn	Si	W	P	S	C
Bal.	16.70	9.85	2.16	1.96	0.96	3.07	0.045	0.030	0.080

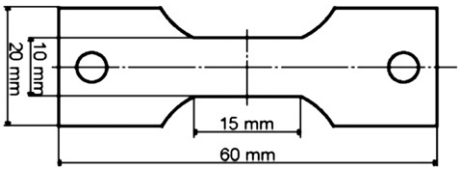

Fig. 1. Shape and sizes of specimens.

Fig. 3 shows the details of the specimen, the specimen holders and the loading device. The specimen was fixed between the holder flanges, and a bending stress with a load of 22.6 N was applied to the specimen by a rod made of 316SS with the tapered and curved end. The maximum tensile stress acting on the bottom surface of the matrix is estimated to be about 100 MPa.

In the process of preparation and start-up, the specimen and holder were immersed in the molten LBE at 200 °C in the crucible. The volume of the liquid LBE was 450 ml. Ar-3%H_2 gas was injected into the LBE to decrease oxygen concentration before heat-up of the LBE to the test temperatures. The LBE temperature was kept around 200 °C for an hour, and then the LBE was heated up to the test temperature of 650 °C. At the same time, the load was applied to the specimen and maintained for 250 h. During the corrosion test, Ar-3%H_2 gas was continuously injected into the LBE. From initial data of the electromotive force (EMF) of the oxygen sensor, oxygen concentration in the LBE was estimated to be 5.2×10^{-8} wt% at the beginning of the corrosion test. Corrosion test conditions are summarized in Table 2. After the test, the residual LBE were removed from the specimen with a glycerin at 160–180 °C and then with a solution containing in volume1/3 of 100% vol CH_3COOH, 1/3 of 30% vol H_2O_2, and 1/3 of 100% vol C_2H_5OH to remove residual LBE on the surface of the specimens for the X-ray diffraction (XRD) analysis.

Before and after the corrosion tests, metallographic examinations of the specimens were performed using a field emission scanning electron microscope (FE-SEM), an energy dispersive X-ray spectrometer (EDX) and an XRD device used with a Cu target.

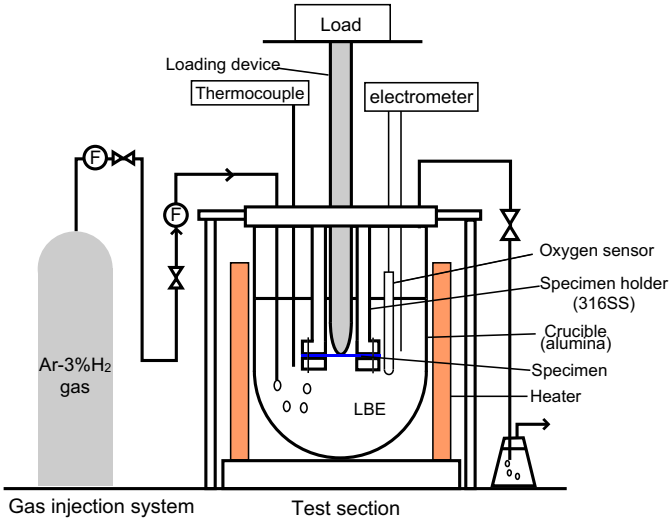

Fig. 2. Experimental apparatus.

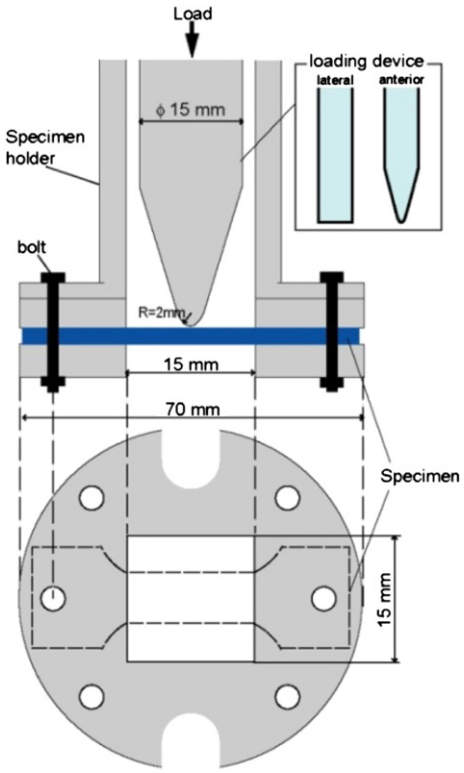

Fig. 3. Details of specimen, specimen holders and loading device.

3. Results

3.1. Before corrosion test

Fig. 4 shows the XRD patterns of Fe–Al alloy-coated specimen before and after the heat treatment. Only the peaks of Fe–Al (ICDD number: 33–20) were observed, which means that the Fe–Al coating layer was in the Fe–Al phase, even though the intensity of some peaks was changed a little.

Fig. 5 shows SEM images of the specimen before the corrosion test: (a) the cross section of the specimen before the heat treatment, (b) the cross section of the specimen after the heat treatment and (c) the EDX results of line analysis performed on the specimen after heat treatment. There is no large difference of the structure of the coating between before and after the heat treatment. Both before and after the heat treatment, the thickness of the coating layers is 20 μm and that of the pre-coating layer is 1 μm. The surface of the coating layer was rough, and the Fe–Al grains are in the form of columns standing normal to the interface between the matrix and the coating layer. The grain size is about 1 μm. The Fe–Al coating layer is dense near the interface between the matrix and the coating layer, while the opening of the Fe–Al grains is wide near the surface of the coating layer. The quantitative analytical results

Table 2
Heat treatment and corrosion test condition.

Temperature of LBE (°C)	650
Test specimens	316SS+Fe–Al
Exposuring time (h)	240
Inert gas	Ar-3%H_2
Load (N)	22.6
Oxygen concentration (wt%)	$<10^{-7}$
Condition of heat treatment	- At 850 °C for 8 h and at 650 °C for 6 h - In Ar gas

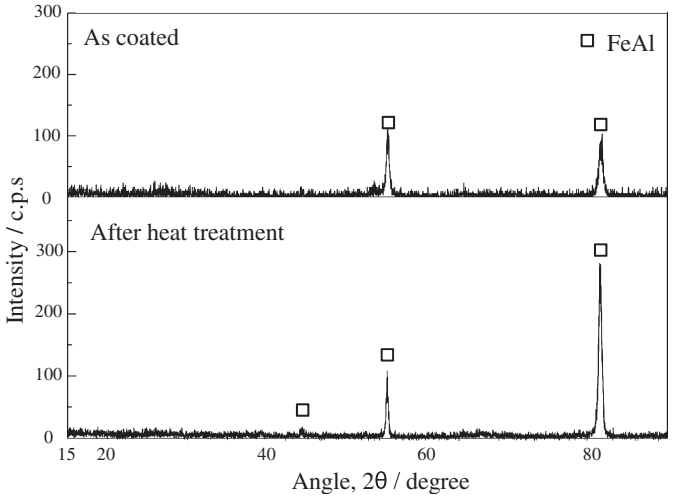

Fig. 4. XRD patterns of specimen surface before and after heat treatment.

of Fe–Al layer before the corrosion test are listed in Table 3. Each analytical points are shown in Fig. 5. The concentration of the coating layer was not changed significantly before and after the heat treatment. As noted above, since the elements contained in 304SS, such as Cr, Ni, Si, Mo and W, were coated at the same time of forming the Fe–Al layer, the coating layer contained these elements. According to the EDX results shown in Fig. 5(c), Al and O increase from the interface between the coating layer and the 316 matrix and at the surface of the coating layer. It can be considered that the Al oxide was formed on the surface of the coating layer and the interface between the coating layer and the matrix. Thickness of these Al oxide scales was 1 μm, respectively.

3.2. After corrosion test

Fig. 6 the XRD patterns of the Fe–Al coated specimen after the corrosion test. Only the peaks of Fe–Al were observed, even though the intensity of some peaks was changed.

Fig. 7 shows the cross section of the specimen after the corrosion test: (a) the whole image of the bent specimen and (b) the detail of the cracked coating layer and the corrosion area in the matrix. The results of the quantitative analysis are listed in Table 4. The coating layer cracked across the layer, though the coating layer dose not crack after the corrosion test without loading (Rivai and Takahashi, 2008). This kind of brittle cracking behavior can be seen in case of oxide scales (Yamaki and Kikuchi, 2010; Schütze et al., 2000). The maximum width of the cracking was 8 μm. LBE penetrated the gaps of the cracks and contacted directly with the matrix. As a result, LBE corrosion occurred around the cracks in the matrix. It is found that the LBE corrosion was severe around the cracks. The three deferent corrosion types could be seen according to the difference of their contrasts. The depth of dissolution corrosion caused by the preferential dissolution of Ni was 10 μm. The detail of these corrosion types are described later. The corrosion was observed along the interface between the Fe–Al coating layer and the matrix. The spalling of coating layer was not observed.

The results of EDX line analysis performed on the coating layer and the corroded area of Fig. 7(b) are shown in Fig. 8: (a) the results performed on from the 316SS matrix to the Fe–Al coating layer and (b) the results performed on the corrosion area. The interface of I, II, III and IV in Fig. 7 (b) means changing the contrast of the picture. As shown in Fig. 8(a), the slightly Ni depletion started at the point which is a little deeper than the interface I. And also Cr depletion started at the same point with Ni. O and Cr increase suddenly at the

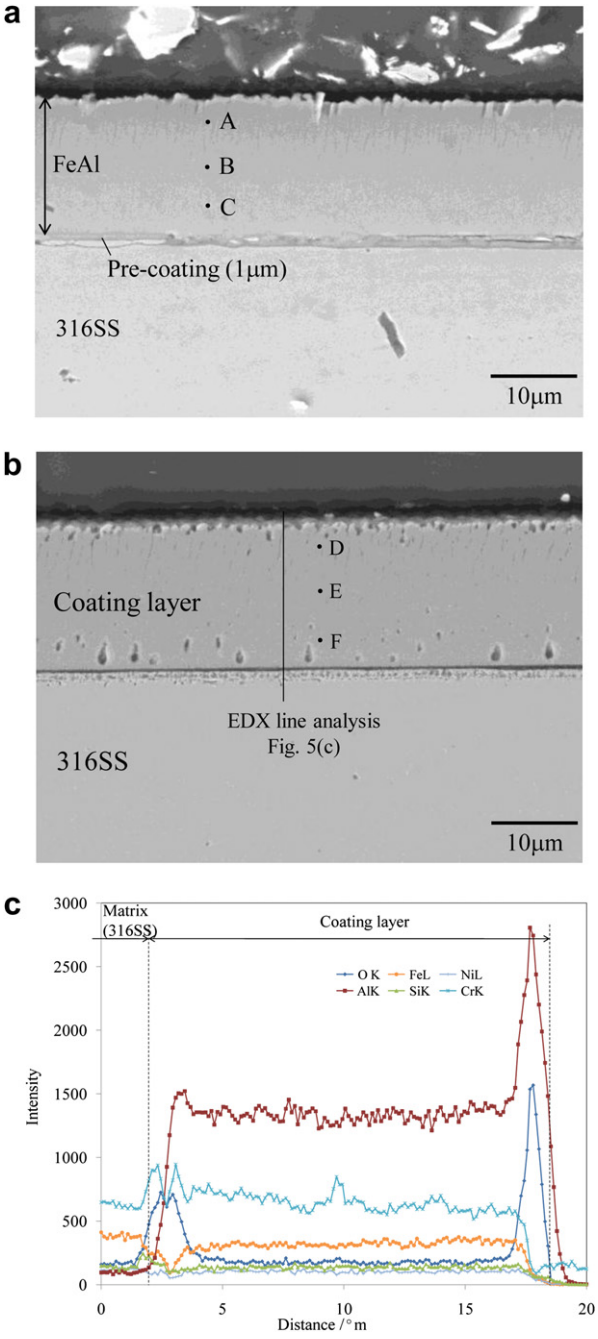

Fig. 5. SEM images of specimens before corrosion test. The results of the quantitative analysis at A–F are listed in Table 3. (a) Cross section of specimen before heat treatment. (b) Cross section of heat-treated specimen. (c) EDX results performed on the specimen after heat treatment. The line are shown in Fig. 5(b).

Table 3
EDX quantitative analytical results of Fe–Al coating layer before corrosion test (wt%). A, B and C were the results measured on the specimen before heat treatment, and D, E and F are on the specimen after heat treatment as shown in Fig. 5 (a) and (b).

	Fe	Al	Cr	Ni	Si	Mo	W
A	52.8	21.2	15.1	6.1	0.9	0.6	3.5
B	51.4	20.3	15.0	6.4	0.9	0.6	5.5
C	50.6	24.0	13.8	5.9	0.9	0.7	3.9
D	56.6	18.3	13.0	6.7	0.8	0.5	4.3
E	56.1	18.8	14.6	6.3	0.8	0.5	3.0
F	53.2	18.9	14.5	6.5	0.8	0.3	5.6

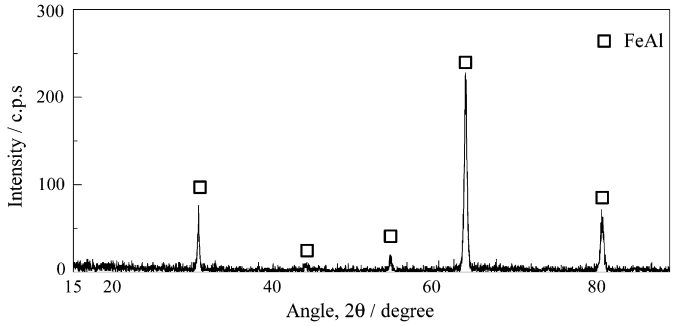

Fig. 6. XRD pattern of coating layer after corrosion test.

interface I. In the area between I and II, O and Cr were measured mainly. Fe increases suddenly at the interface II, and Fe and O were measured mainly in the area between II and III. It is considered that the 316 matrix was oxidized and Cr oxide and Fe oxide was formed. At the interface III, Al and O increase suddenly. This fact indicates that Al oxide was formed between the coating layer and the matrix. Thickness of the Al oxide is 1 μm. It can be considered that this Al oxide was formed on the specimen before the corrosion test since thickness Al oxide was not changed. After the distance of 9 μm, Al and other element don't change significantly. From Fig. 8(a), slightly depletion of Ni and Cr were measured before the interface IV. Cr and O were observed between the interface IV and V, and Fe and O were observed after the interface V. These facts also indicate that the Cr oxide and Fe oxide were formed on the matrix, respectively.

According to all results as explained above, cracking caused by the loading and the LBE corrosion were seen. The types of LBE corrosion, which could be seen in this study, can be explained as follows:

1. Dissolution of the elements from the 316 matrix to LBE. The preferential dissolution of Ni and Cr were strong, the maximum depth of Ni and Cr dissolution were 15 μm.
2. Oxidation of 316 matrix caused by oxygen in the liquid LBE. Two kinds of oxide were exhibited; the deeper oxide was Cr oxide, and the other was Fe oxide. The maximum thickness of Cr oxide was 3 μm, and the mean thickness was 2 μm. The maximum thickness of Fe oxide was 4 μm, and the mean thickness was 2 μm.

4. Discussion

4.1. Cracking and strain

It is considered that the cracking of the coating layer mainly caused by the loading. The thermal expansion coefficients of Fe–Al and 316SS are approximately same (Fe-40%atAl: 21.0 × 10^{-6}/°C, 316SS: 21.0 × 10^{-6}/°C, the temperature range of 0–600 °C). Therefore, it is difficult to observe the influence of thermal expansion of the layer. The present coating layer of Fe–Al alloy consisted of columnar crystal grains normal to the surface of the steel as in the result of Lui et al. (Lui et al., 1998). Fig. 5 shows that the surface of the coating layer after the heat treatment was rough, and there were opening of columnar grain interfaces which were larger near the surface than in deeper area. These opening between adjacent crystal grains might cause the brittle cracking across the coating layer.

From the image of the cross section shown in Fig. 7, the strain in the fractured coating layer ε which is parallel to the circumferential strain were estimated by

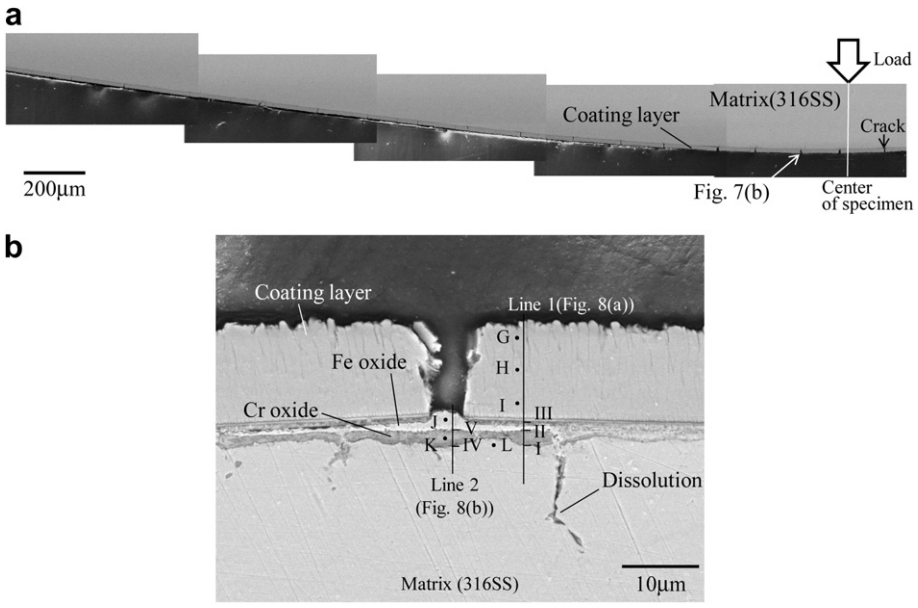

Fig. 7. SEM images of specimen after corrosion test. The results of the line analysis are shown in Fig. 8, and the results of the quantitative analysis are listed in Table 4. (a) Whole image of the observed side after corrosion with loading. (b) Cross section of cracked layer after corrosion with loading.

$$\varepsilon = \frac{d_{\text{width}}}{d_{\text{interval}} + d_{\text{width}}} \quad (1)$$

where d_{width} is the width of the crack and d_{width} is the interval between the cracks as defined in Fig. 9(a). The distribution of ϵ is shown in Fig. 9(b). The zero in the horizontal axis is the center of the specimen shown in Fig. 7(a). It can be considered that the maximum 6.5% of tensile strain applied to the coating layer.

4.2. Corrosion behavior of 316 matrix and Fe–Al coating layer

The dissolution corrosion caused by the preferential dissolution of the elements from the 316 matrix into the liquid LBE and the oxidation were exhibited on the 316 matrix. The dissolution corrosion rates of 316 type austenitic steel in LBE at 600 °C, which were reported in the reference papers, are listed in Table 5. The oxygen concentrations of LBE used in the literatures were approximately same. There are no reports which obtain the corrosion rate at 650 °C calculated with corrosion data obtained from the results for several corrosion durations. The corrosion rates listed in Table 5 were calculated assuming that the corrosion was controlled by the linear kinetics. In case of the corrosion duration of 250 h, the corrosion depth can be supposed 10–26 μm by the referenced corrosion rates. In this study, the maximum dissolution depth of 316SS matrix was 15 μm. It is same or smaller than the

Table 4
EDX quantitative analytical results of Fe–Al coating layer and corroded area after corrosion test (wt%). G, H and I were the results measured on the coating layer, and K and L were on the corroded area.

	Fe	Al	Cr	Ni	Si	Mo	W	O	Zn
G	57.5	19.8	13.4	6.0	0.7	–	2.6	–	–
H	58.9	19.2	12.4	5.8	0.8	–	2.9	–	–
I	54.8	19.4	15.5	6.9	0.6	–	2.9	–	–
J	92.4	–	1.74	5.12	–	0.7	–	–	–
K	11.1	–	37.0	–	1.78	5.67	–	26.6	17.7
L	84.4	–	6.9	3.6	0.8	2.4	1.8	–	–

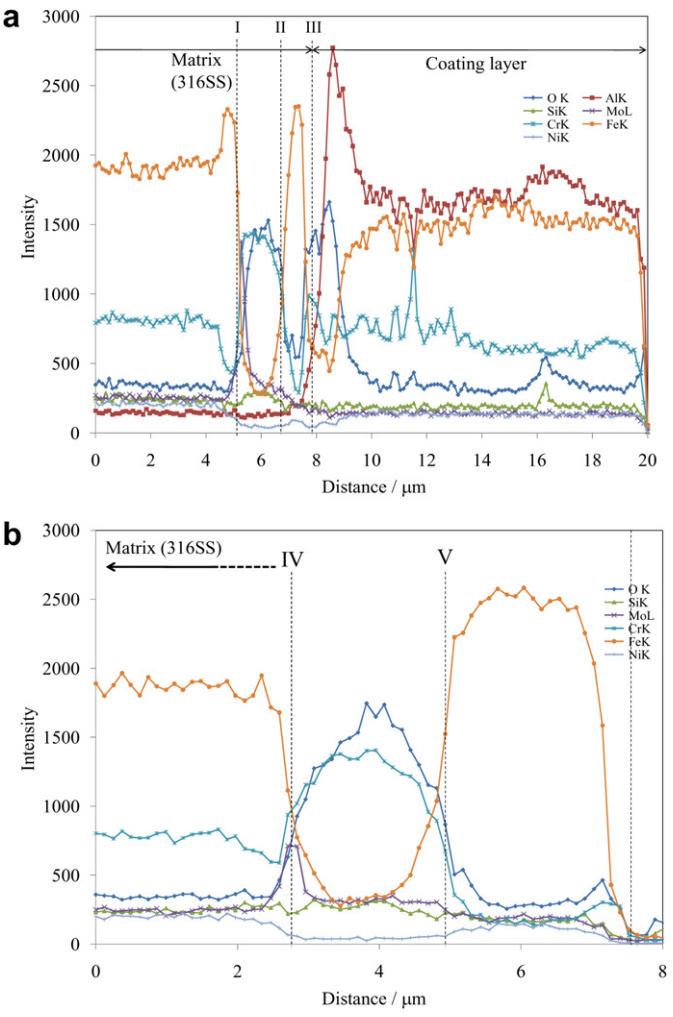

Fig. 8. EDX results of corroded area which are shown in Fig. 7(b). (a) Line 1. (b) Line 2.

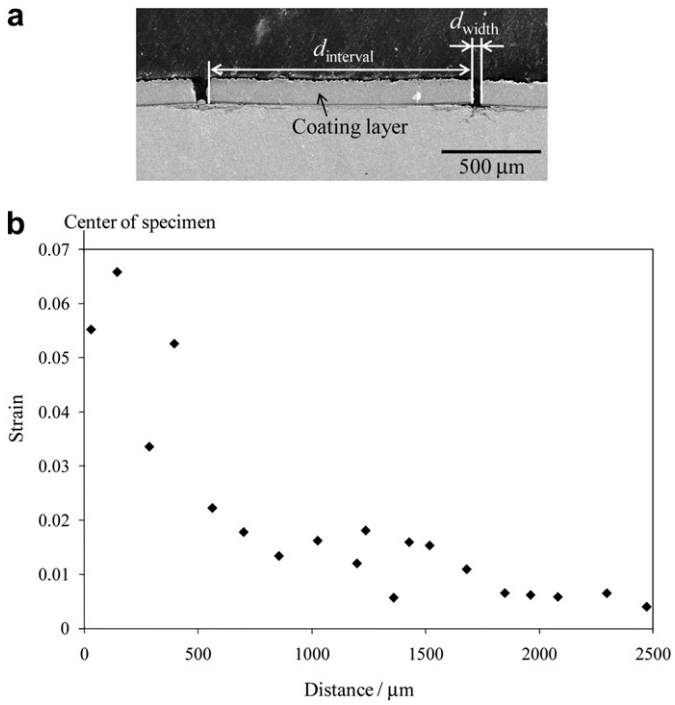

Fig. 9. Strain distribution at surface of coating layer. The strain was calculated with the width and the interval of the cracking at the surface of the coating layer by the cross section of the specimen. (a) Definition of strain calculated with width and interval of cracking. (b) Strain distribution.

values of the literature, even though the corrosion temperature of this study was 50 °C higher than it of the literatures. This fact indicates that the corrosion rate became lower, or the coating layer didn't crack at the beginning of the corrosion duration. The dissolution corrosion proceeds to not only the depth direction but also the surface direction (Sapundjiev et al., 2006). Especially, the corrosion rate to the surface direction may be higher than that to the depth direction. After 250 h of the corrosion duration, almost all surfaces of 316L samples were corroded. Since the coating layer prevented to contact the 316SS matrix with the liquid LBE, the dissolution corrosion of the matrix to the surface direction could be reduced.

The corrosion in the 316 matrix exhibited along the interface between the coating layer and the 316SS matrix. It can be considered that this behavior caused by the corrosion of the pre-coating layer. The pre-coating layer is the weakest to LBE corrosion attack of three layers because it was produced with only type 304 stainless steel target containing Ni which had the highest solubility in LBE. Since the pre-coating layer dissolves more easily than Fe—Al alloy layer and the matrix, the damage of dissolution corrosion can occur at high temperature. The corrosion of the pre-coating layer

Table 5
Corrosion rate of 316L in LBE obtained in the literatures. The corrosion rates were calculated assuming that the dissolution corrosion is controlled by the linear kinetics.

Ref.	Test type	Temperature (°C)	Oxygen concentration (wt%)	Corrosion rate (μm year^{-1})
Martín et al., 2004	Stagnant	600	8×10^{-6}	963.6
Soler et al., 2004	Stagnant	600	$<10^{-7}$	367.9
Deloffre and Terlain, 2004	Stagnant	600	8×10^{-10}	613.2

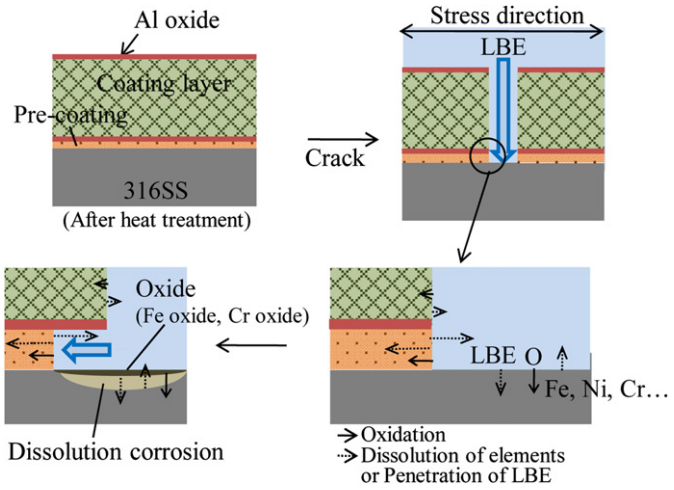

Fig. 10. Schema of the corrosion mechanism of the coated specimen with cracks of the coating layer.

promotes the penetration of LBE into the interface between the matrix and the coating layer.

The Fe—Al coating layer was not corroded by LBE even though the coating layer contains Ni, Cr, Fe and Al which have high solubility into LBE. As Müller et al. reported, the thin Al oxide has good protection to the LBE corrosion (Müller et al., 2000). The Al oxide was formed on the surface of the coating layer after the heat treatment process. It can be considered that the protection of this thin Al oxide is one of the reasons why the coating layer is not corroded by LBE.

4.3. Cracking and corrosion mechanism of coating layer and 316SS matrix

Fig. 10 shows the schema of the corrosion mechanism of the coated specimen with cracks of the coating layer. The dissolution corrosion of 316SS starts driven by the preferential dissolution of Ni. In case of the corrosion of the specimen without the coating layer, all surface of the 316SS specimen contact with LBE, and Ni can dissolve into the liquid LBE from any surface of the specimen. On the other hand, in case of with coating layer, the 316SS specimen don't contact with LBE directly. If the coating layer cracks, LBE can come into the cracks and contact the 316SS matrix. Therefore, the dissolution corrosion can start around the cracks. The oxidation of the 316SS matrix is caused by the oxygen dissolved in LBE. The oxidation can also start after contacting the matrix with LBE which come into the cracks. Where the coating layer doesn't crack, the liquid LBE cannot contact with the matrix, and the corrosion cannot start. Therefore, proceeding of the corrosion to the surface direction can be reduced by the coating layer. Moreover, the pre-coating layer is the weakest to LBE corrosion attack of three layers because it was produced with only type 304 stainless steel target containing Ni which had the highest solubility in LBE. Since the pre-coating layer dissolves more easily than Fe—Al alloy layer and the matrix, the damage of dissolution corrosion can occur. The gaps between the matrix and the coating layer were caused by the dissolution of the pre-coating layer. The corrosion of the pre-coating layer promotes the penetration of LBE into the interface between the matrix and the coating layer. Therefore the LBE corrosion occurs in the matrix and the pre-coating layer.

5. Conclusion

The corrosion test was performed for austenitic steel 316SS with Fe–Al alloy coating in LBE at 650 °C under loading for immersion time of 250 h. From the results, it can be concluded as follows:

1. The coating layer was not corroded by LBE, but cracked. The LBE penetrated into the cracks and corroded the 316SS matrix and the pre-coating layer. The matrix was corroded along the interface between the matrix and the pre-coating layer because of the LBE penetration through the corroded zone of the pre-coating layer.
2. The matrix exhibited the dissolution corrosion caused by the preferential dissolution of Ni and the oxidation forming the Fe oxide and Cr oxide.
3. The coating layer is effective to reduce the surface of the matrix to be corroded by LBE, and can moderate the corrosion of the depth direction.

Acknowledgments

The authors wish to thank Mr. Kitayama of The Advanced Materials Processing Institute Kinki Japan for producing of coating by UBMS method.

References

Deloffre, Ph., Terlain, A., 2004. Influence of Zn as a spallation product on the behaviour of martensitic steel T91 and austenitic steel 316L in liquid Pb–Bi. J. Nucl. Mater. 335, 244–248.

Kurata, Y., Futakawa, M., Saito, S., 2004. Corrosion behavior of Al-surface-treated steels in liquid Pb–Bi in A Pot. J. Nucl. Mater. 335, 501–507.

Kurata, Y., Futakawa, M., Saito, S., 2005. Comparison of the corrosion behavior of austenitic and ferritic/martensitic steels exposed to static liquid Pb–Bi at 450 and 550 °C. J. Nucl. Mater. 343, 335–340.

Lui, Z., Gao, W., Wang, F., 1998. Oxidation behavior of Fe–Al intermetallic coating produced by magnetron sputter deposition. Scr. Mater 39, 1497–1502.

Martín, F.J., Soler, L., Hernández, F., Gómez-Briceño, D., 2004. Oxide layer stability in lead–bismuth at high temperature. J. Nucl. Mater. 335, 194–198.

Müller, G., Schumacher, G., Zimmermann, F., 2000. Investigation on oxygen controlled liquid lead corrosion of surface treated steels. J. Nucl. Mater. 278, 85–95.

Rivai, A.K., Takahashi, M., 2008. Compatibility of surface coated steels, refractory metals and ceramics to high temperature lead-bismuth eutectic. Prog. Nucl. Energy 50, 560–566.

Sapundjiev, D., Van Dyck, S., Bogaerts, W., 2006. Liquid metal corrosion of T91 and A316L materials in Pb–Bi eutectic at temperatures 400–600 °C. Corros. Sci. 48, 577–579.

Schütze, M., Ito, S., Przybilla, W., Echsler, H., Bruns, C., 2000. Test methods and data on the mechanical properties of protective oxide scales, High-Temperature Corros. Prot. 2000. 19–30.

Soler, L., Martín, F.J., Hernández, F., Gómez-Briceño, D., 2004. Corrosion of stainless steels in lead–bismuth eutectic up to 600 °C. J. Nucl. Mater. 335, 174–179.

Yamaki, E., Kikuchi, K., 2010. A stability of oxide layers formed in LBE on HCM12A to external loading. J. Nucl. Mater. 398, 153–159.